X-ray Absorption Spectroscopy Study of the Hydrogen Bond Network in the Bulk Water of Aqueous Solutions

Lars-Åke Näslund,[†,‡] David C. Edwards,[§] Philippe Wernet,[‡,||] Uwe Bergmann,[‡] Hirohito Ogasawara,[‡] Lars G. M. Pettersson,[†] Satish Myneni,[⊥] and Anders Nilsson*[,†,‡]

Fysikum, AlbaNova, Stockholm University, SE-106 91 Stockholm, Sweden, Stanford Synchrotron Radiation Laboratory, P.O. Box 20450, Stanford, California 94309, U.S.A., Department of Chemistry, Princeton University, Princeton, New Jersey 08544, U.S.A., BESSY, Albert-Einstein-Strasse 15, D-12489 Berlin, Germany, and Department of Geosciences, Princeton University, Princeton, New Jersey 08544, U.S.A.

Received: January 24, 2005; In Final Form: April 21, 2005

We utilized X-ray absorption spectroscopy (XAS) and X-ray Raman scattering (XRS) in order to study the ion solvation effect on the bulk hydrogen bonding structure of water. The fine structures in the X-ray absorption spectra are sensitive to the local environment of the probed water molecule related to the hydrogen bond length and angles. By varying the concentration of ions, we can distinguish between contributions from water in the bulk and in the first solvation sphere. We show that the hydrogen bond network in bulk water, in terms of forming and breaking hydrogen bonds as detected by XAS/XRS, remains unchanged, and only the water molecules in the close vicinity to the ions are affected.

1. Introduction

The interaction between ions and water molecules influences macroscopic properties of water, for example, boiling point, freezing point, surface tension, and viscosity. It also affects other important properties in many chemical and biological processes. In electrochemical processes, the rate of charge transfer is controlled by the mobility of the ions in solutions.[1] Within the living body, even a small amount of ions influences the conformation of proteins and nucleic acid strands and their functions.[2,3]

It is generally assumed that the interactions between water and ions, which result in effects on the macroscopic properties, affect the long range ordering of the hydrogen bonding network in the bulk liquid, for example, by breaking or forming hydrogen bonds (HB). The magnitude of the effect follows the Hofmeister series given in Chart 1.[4,5]

In connection to measured macroscopic properties of aqueous solutions, ions that exhibit strong interactions with water molecules, for example, small di- and/or trivalent ions, are often called structure breakers, while ions that exhibit weaker interactions with water than water itself, for example, large monovalent ions, are called structure makers. Another view, which gives an opposite definition of the structure-maker/structure-breaker concept, is the correlation to the Jones−Dole viscosity *B* coefficient;[6] a positive (negative) *B* coefficient in the Jones−Dole expression of viscosity indicates increased (reduced) viscosity relative to pure water.[7] Strongly hydrated ions give positive *B* coefficients and are thus called structure makers, while weakly hydrated ions reduce the viscosity leading to a negative *B* coefficient and are called structure breakers. A third approach to the structure-breaker/structure-maker concept is based on the effect on the entropy of ion solvation, which also has been considered to indicate water structuring.[8] By separating the entropy into ion and hydration water contributions, the latter can describe the change in entropy of the water due to the presence of ions. The structure makers have negative hydration entropy, whereas the structure breakers increase the entropy associated with the hydration waters.

The structure-breaker/structure-maker nomenclature is thus ambiguous and is based on macroscopic observations. The important result is, however, that strongly hydrated ions affect the properties of the liquid.

Recent neutron diffraction studies of water in ionic solutions suggest that a strongly hydrated ion increases the difference between the HB donating and accepting capacity of the linked water molecules, resulting in a breakdown of the HB network (i.e., an effect similar to increased temperature or pressure).[9] The effect on the pair-correlation functions from the presence of ions is, however, only seen for very concentrated solutions where most water molecules are within the first or second coordination spheres. Recent time-resolved infrared spectroscopy studies of the rotational dynamics of water by Omta et al.[10,11] also indicated that the ions affect only the water molecules in the first coordination sphere. Moreover, molecular dynamics (MD) simulations have not provided a clear, conclusive result regarding the effects of ions on the HB network in the bulk liquid. Both supportive and negative pictures of the structure-maker/-breaker concepts have been obtained.[12−18]

In previous work, we have used X-ray absorption spectroscopy (XAS) and X-ray Raman scattering (XRS) at the oxygen K edge (O 1s) to demonstrate the ability to probe the HB structure in liquid bulk water.[19−22] The comparison between liquid water and ice showed a large difference in the spectral features related to specific hydrogen-bonded configurations. The O 1s XA spectrum of bulk ice has a pronounced structure around 541 eV (post-edge), while the ice surface and liquid water have additional strong spectral features seen as a pre-edge peak at

* Corresponding author. Phone: +1 (650) 926 2233. Fax: +1 (650) 926 4100. E-mail: nilsson@slac.stanford.edu.
[†] Stockholm University.
[‡] Stanford Synchrotron Radiation Laboratory.
[§] Department of Chemistry, Princeton University.
[||] BESSY.
[⊥] Department of Geosciences, Princeton University.

10.1021/jp050413s CCC: $30.25
Published on Web 06/16/2005

CHART 1: Hofmeister Series

Strongly hydrated anions — weakly hydrated anions

$SO_4^{2-} > HPO_4^{2-} > F^- > Cl^- > Br^- > I^- > NO_3^- > ClO_4^-$

$NH_4^+ > Cs^+ > Rb^+ > K^+ > Na^+ > Ca^{2+} > Mg^{2+} > Al^{3+}$

weakly hydrated cations — strongly hydrated cations.

535 eV and an enhancement at 537 eV (main-edge); these features are related to broken or weakened donating H-bonds that generate an asymmetry compared to the near-tetrahedral symmetry in bulk ice.[19−21] The post-edge peak at 541 eV was assigned to OH groups that are involved in a donating HB, while the pre-edge peak at 535 eV and the main-edge peak at 537 eV were assigned to OH groups that are either weakly or not hydrogen-bonded.[20] In ice, the post-edge intensity is large, since both OH groups are involved in donor hydrogen bonds. Results in previous works indicate that the asymmetric or unsaturated donating HB configuration, also denoted the single-donor (SD) configuration, applies to a dominating fraction of the water molecules.[19,20] In the present paper, we evaluate the effect of ions on the HB network in aqueous solutions through analysis of the O 1s XA spectra. Although XAS and XRS only are sensitive to the local environment (i.e., the first and second hydration spheres of the probed water molecule), the techniques probe all water molecules simultaneously in the sample with equal probability. The recorded XA spectrum is thereby a sum of contributions from all the probed water molecules, and a change in the number of hydrogen bonds induced by the ions is therefore reflected in the fine structure of the XA spectrum. However, the spectroscopies are less sensitive to structural changes that do not involve breaking or forming hydrogen bonds. If ions break down the HB network in bulk water (i.e., break hydrogen bonds), we expect a spectral signature indicating more broken or weakened hydrogen bonds. In particular, we should see an increase in the pre- and main-edge intensities at 535 and 537 eV, respectively, and a simultaneous decrease in the post-edge intensity around 540 eV.[20,23] If ions induce an increase of the fraction of tetrahedrally coordinated molecules in the bulk water, we expect to see the reverse. By comparing XA spectra for water with and without ions, the ion hydration effect on the HB network in the form of breaking or forming hydrogen bonds in the bulk water may thus be obtained.

2. Experimental Section

The near-edge region of XAS, also known as near-edge X-ray absorption fine structure (NEXAFS) or X-ray absorption near edge structure (XANES), has been increasingly used as a direct probe for the unoccupied electronic states of molecules in the last few decades. The growth in the number of applications of this technique has been closely connected to the development of synchrotron radiation sources at national laboratories. Consequently, near-edge XAS is now a widely used technique for elucidating the nature of bonding between molecules, in interfaces, and of adsorbates.[24] However, application of this technique to oxygen K edge measurements of aqueous solutions is challenging because of the incompatibility of the high vapor pressure of the liquid with the vacuum environment required by the soft X-ray beamline. Development of intense third-generation synchrotron light sources, effective differential pumping systems, and the possibility to make ultrathin, soft X-ray transparent windows to separate the ultrahigh vacuum in the beamline from an ambient atmosphere in a high-pressure cell have, however, made soft X-ray-based measurements of aqueous solutions possible.[19,23,25−29]

2.1. The XAS Fluorescence Yield Experimental Technique. XAS fluorescence yield measurements were performed at the soft X-ray endstation for environmental research (SXEER); see Figure 1. SXEER is designed to separate the sample chamber from vacuum in the synchrotron beamline and was, for the aqueous solution experiments, connected to beamline 8.0 at the Advanced Light Source (ALS) in Berkeley, CA. A differential pumping system between the ultrahigh vacuum in the beamline and the sample chamber makes it possible to use

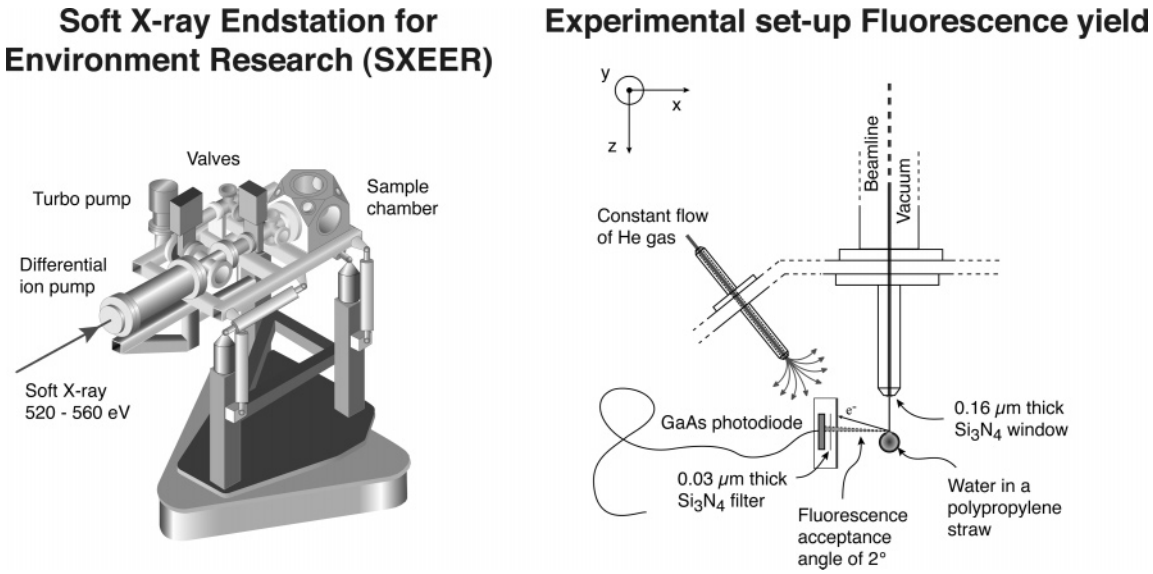

Figure 1. Left: The soft X-ray endstation for environmental research (SXEER). Synchrotron beamline endstation used for O 1s X-ray absorption spectroscopy of liquid water and aqueous solutions. Right: The experimental setup in the sample chamber of SXEER gives an ambient environment with atmospheric pressure and room temperature.

a 0.16-μm-thick silicon nitride (Si_3N_4) window as a separator. The chamber could then be filled with helium gas (1s binding energy of 24.6 eV) that kept the liquid sample under atmospheric pressure and room temperature.

The aqueous solutions were placed in a vertically mounted polypropylene straw, 25 mm long and 8 mm in diameter. Along the straw, from the top, there was a 10-mm-long and 1-mm-wide slot. With this arrangement, a stable liquid surface with low curvature could be exposed to the beam. Vaporization of the aqueous samples occurred during measurement, especially since there was a constant flow of dry helium gas through the chamber that continuously removed the water vapor. However, because of the design of the straw, the position and the form of the probed water volume were independent of the evaporation, since the vaporized liquid was continuously replaced with fresh solution. Recording a spectrum took about seven minutes, and the change in concentration because of the vaporization was shown to be negligible on that time scale.

The absorption spectrum was recorded indirectly by detecting fluorescence photons from the core-hole decay process. The detector was a sensitive gallium arsenide (GaAs) photodiode and was placed perpendicular to the incoming photon beam; see Figure 1. The geometry of the sample setup, with respect to incoming and emitted X-rays, is very important in order to avoid saturation effects.[30,31] Saturation is reduced by maximizing the penetration depth of the X-ray beam by letting the X-ray photons impinge on the sample normal to the surface and by minimizing the detection depth by collecting the fluorescence at a grazing angle. A 0.4-mm-wide metal aperture was placed in front of the detector to reduce the acceptance angle to only 2°. A 30-nm-thick Si_3N_4 film was placed between the metal aperture and the photodiode to protect the diode from charged particles, low energy photons from the He gas, and possible photons from electronic transitions in the valence states of the sample.

The recorded signal had contributions from three sources: fluorescence from the liquid sample, fluorescence from gas-phase water, and thermal background (dark current). The dark current intensity was subtracted from the spectra by assuming a linear contribution with a slope defined by the slope of the spectra in the energy range 520−525 eV. To correct for photon flux variations, each spectrum was normalized to the incident photon intensity, I_0, which was monitored with a gold mesh in the beamline. The I_0-normalized spectra were thereafter normalized with an absorption spectrum of the Si_3N_4 window that separated the helium atmosphere from the vacuum in the beamline. This was necessary because of adsorbed water molecules on the window. The spectra were calibrated in absolute energy using the peak positions of the gas-phase water contributions as a reference. Finally, the gas-phase contributions were subtracted, and the corrected spectra were normalized by area between 530 and 550 eV. Figure 2 demonstrates the steps involved to obtain the final XAS spectra.

2.2. Energy Calibration for the XAS Measurements. Calibration of the absolute energy of the incident X-rays is not trivial. It can, for example, be accomplished through the use of a well-known reference sample. Photon energy calibration of the XA spectrum of gas-phase water could be performed with peak positions known from electron energy loss spectroscopy (EELS) studies,[32,33] where the absolute energies were calibrated with respect to the elastically scattered peak. Since this method is subject to uncertainties, we used an alternative method. A mixture of gas-phase water ($H_2O(g)$), molecular oxygen ($O_2(g)$), and helium (He) was kept in the chamber under atmospheric pressure and ambient temperature. The O 1s XA spectrum of the gas mixture was thus a combination of contributions from $H_2O(g)$ and $O_2(g)$, and since the O_2 and H_2O peaks are well-separated, the spectrum can be energy-calibrated by the O_2 peak position from earlier measurements on the O_2 molecule physisorbed on graphite[34] and Pt(111)[35] (note that the XA spectra of free $O_2(g)$[36] and physisorbed O_2[34,35] have identical shapes). The peak position of the physisorbed O_2 is calibrated by determining spectroscopic features of the substrate using first- and second-order light with the aid of an electron spectrometer.[37] The difference between the kinetic-energy positions recorded with first- and second-order light gives the correct photon energy. The gas-phase water spectrum was thus calibrated with respect to this. A comparison of the energy positions of the gas-phase water peaks from EELS[32] with our XAS measurements shows a positive energy shift of 0.2 eV; see Table 1.

In the recorded spectra of liquid water or aqueous solutions, which also had contributions from gas-phase water, the third gas-phase peak, the O 1s transition into the first Rydberg orbital, is sharp and was easily detected. By knowing its energy position of 537.25 eV (Table 1), each spectrum could thus be shifted to the correct energy. All the aqueous solution spectra are thereby energy-calibrated and directly comparable.

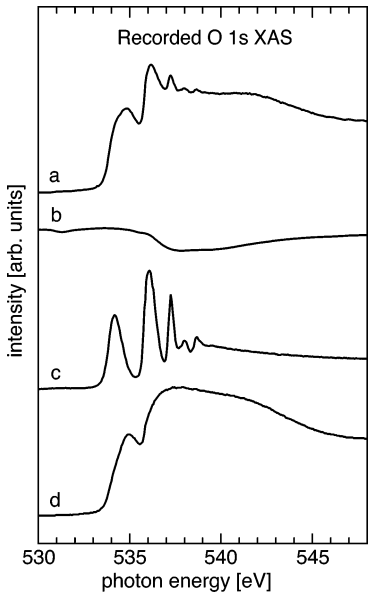

Figure 2. X-ray absorption spectra of (a) the sample (pure water), (b) the Si_3N_4 window, (c) water vapor, and (d) the result after normalization to the window transmission function (b) and subtraction of gas-phase contribution (c). The spectrum from the sample has contributions from the water vapor in the He atmosphere. Normally, the peaks are smaller than shown in the figure, and it is possible to record spectra without water vapor peaks. However, without the vapor peaks, it is difficult to calibrate the photon energy. See text for details about the correction of the spectra.

TABLE 1: The Gas-Phase Spectrum Exhibits Well-Separated Peaks Corresponding to O 1s Excitations into the Antibonding O−H $4a_1$ and $2b_1$ Molecular Orbitals at Low Energies (534 and 536 eV) and Transitions into the Rydberg Orbitals at Higher Energies[38,39]

		peak position/[eV]	
peak no.	transition	EELS[a]	XAS[a]
A	$1a_1 \rightarrow 4a_1$	534.0	534.20
B	$1a_1 \rightarrow 2b_1$	535.9	536.10
C	$1a_1 \rightarrow 3pb_2 + 3pa_1$ Rydberg orbitals	537.1	537.25

[a] Excitation energies measured by EELS[32] and XAS.

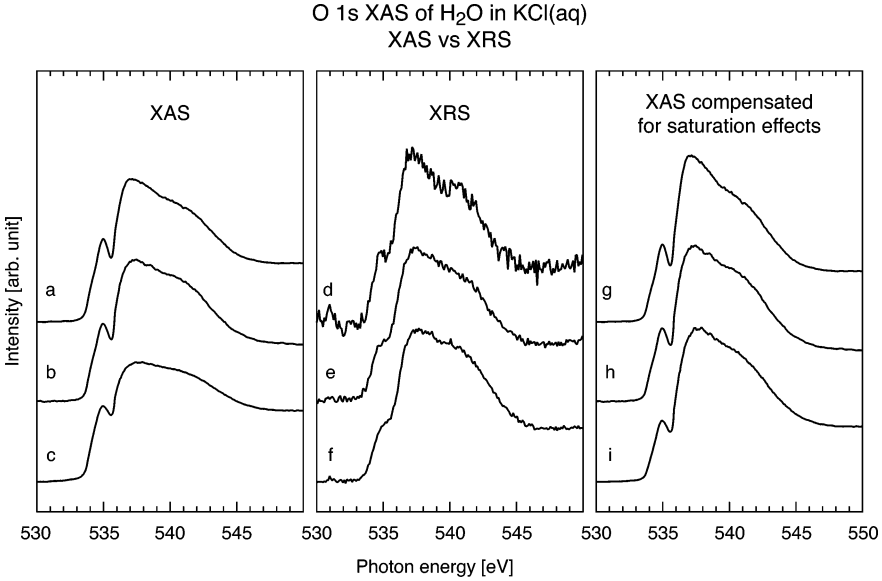

Figure 3. O 1s X-ray absorption spectra of (a) 4 m KCl(aq), (b) 1 m KCl(aq), and (c) pure water, as recorded with XAS, (d) 4 m KCl(aq), (e) 1 m KCl(aq), and (f) pure water, as recorded with XRS. The rightmost panel shows corresponding XAS spectra after compensation for saturation: (g) 4 m KCl(aq), (h) 1 m KCl(aq), and (i) pure water.

2.3. Saturation Effects in the XAS Measurements. The sample geometry of the XAS experiment, with incoming X-rays normal to the sample surface and grazing angle fluorescence detection, was optimized to reduce saturation effects as much as possible. Unfortunately, because of the strong X-ray absorption (i.e., high absorption cross-section), saturation effects turned out to be impossible to eliminate completely. A comparison between the XAS and the XRS spectra of pure water, 1 m KCl(aq) and 4 m KCl(aq), shows that a normal-incidence-grazing-detection geometry is not enough to completely remove saturation effects in the XAS measurements; see Figure 3. However, it has been shown that saturated XA spectra can be compensated for saturation effects by applying a correction procedure.[30,31,40−43] If the sample composition and sampling depth are known, a saturation compensating factor can be calculated from the extended X-ray absorption region. However, this procedure is very sensitive to any possible errors in the measured slope of the ionization continuum in the extended XAS region. We have therefore chosen an alternative approach by using the XRS spectra, which are inherently free from saturation effects, as reference in the compensation procedure.

The theoretical description of the fluorescence yield signal dI_f from a bulk sample is[24]

$$dI_f(\theta, h\nu) = \frac{\Omega}{4\pi} I_0 A_0 \omega_f \mu_x(\theta, h\nu)\, e^{-\mu_x(\theta, h\nu)z}\, e^{-z/D(\epsilon_f)}\, dz \quad (1)$$

where θ is the angle between the incident X-rays and the surface of the sample, Ω is the solid angle for the emitted fluorescence, I_0 is the incident photon flux density, A_0 is the X-ray exposed area, ω_f is the fluorescence yield efficiency, μ_x is the linear absorption coefficient, $D(\epsilon_f)$ is the effective escape depth of the fluorescence with energy ϵ_f, and z is the depth to the increment dz where the fluorescence photon is emitted. Integration over the sample thickness, which is much thicker than the photon penetration depth, gives the measured intensity

$$I_f(\theta, h\nu) = \frac{\Omega}{4\pi} I_0 A_0 \omega_f \frac{\mu_x(\theta, h\nu)}{\mu_x(\theta, h\nu) + 1/D(\epsilon_f)} \quad (2)$$

The experimental setup had a fixed geometry, and the recorded signal is normalized to I_0. Equation 2 can therefore be simplified

$$\frac{I_f(h\nu)}{I_0} = C\frac{\mu_x(h\nu)}{\mu_x(h\nu) + 1/D(\epsilon_f)} \quad (3)$$

If $D(\epsilon_f)$ (in centimeters) is sufficiently small, that is, $1/D(\epsilon_f) \gg \mu_x$, the recorded signal is proportional to $\mu_x(h\nu)$ (in reciprocal centimeters), which is our aim with XAS. But if $D(\epsilon_f)$ is large (e.g., when the fluorescence is detected normal to the surface),[24] eq 3 becomes equal to the constant C, that is, all photons are absorbed within the detection depth, and thus, no spectral features can be observed. At intermediate values of $D(\epsilon_f)$, the spectral features become suppressed, and the recorded spectrum is saturated (see, e.g., Figure 3 in Guo et al.[26]). When the fluorescence is detected at an angle δ from the surface normal, the escape depth is related to the X-ray absorption coefficient according to

$$D(\epsilon_f) = \frac{\cos\delta}{\mu_x(\epsilon_f)} \quad (4)$$

Thus, grazing angle detection (δ close to 90°) will reduce the fluorescence escape depth and thereby also the saturation effect. In our case with a highly concentrated sample, this is not enough, and the signal needs to be compensated for the reduced intensity by a factor $S(\epsilon_f)$

$$S(\epsilon_f)\frac{I_f(h\nu)}{I_0} = C\frac{\mu_x(h\nu)}{\mu_x(h\nu) + 1/D(\epsilon_f)} \quad (5)$$

The linear absorption coefficient can then be calculated

$$\mu_x(h\nu) = \frac{\dfrac{S(\epsilon_f)}{CD(\epsilon_f)}\dfrac{I_f(h\nu)}{I_0}}{\left[1 - \dfrac{S(\epsilon_f)}{C}\dfrac{I_f(h\nu)}{I_0}\right]} \quad (6)$$

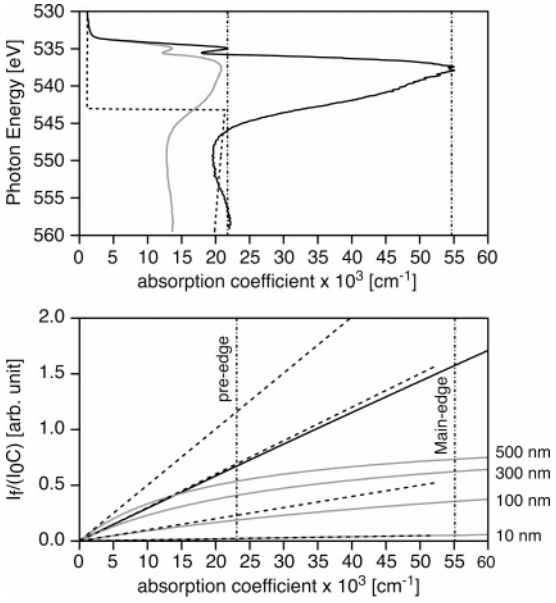

Figure 4. (a) The saturated XAS spectrum (solid gray) compared to the corrected spectrum (solid black) normalized to the tabulated values for the oxygen absorption edge[45] (dotted). The dash−dotted lines indicate the value of the absorption coefficient at the pre-edge and the main-edge peak: 21 700 and 54 600 cm^{-1}, respectively. (b) The dotted lines indicate the correct linear intensity−absorption relationship for each case of detection depths. The solid gray lines are the saturated intensity−absorption relationship for the detection depths 10, 100, 300, and 500 nm, respectively. Increasing detection depth leads to higher degree of saturation effects. In the current XAS measurements of the aqueous solutions, the detection depth is ca. 300 nm.[44] The gray solid line corresponding to the 300 nm detection depth can, however, be compensated for the saturation effects, which is indicated by the solid black line. The dash−dotted lines indicate the expected value of the absorption coefficient at the pre-edge and the main-edge peak for the saturated spectrum: 23 100 and 55 100 cm^{-1}, respectively.

or simply

$$\mu_x(h\nu) = \frac{C'(\epsilon_f)\dfrac{I_f(h\nu)}{I_0}}{\left[1 - C''(\epsilon_f)\dfrac{I_f(h\nu)}{I_0}\right]} \qquad (7)$$

where $C'(\epsilon_f)$ is a scaling factor and $C''(\epsilon_f)$ is the saturation compensating factor.

In Figure 3, we compare XAS and XRS spectra of pure water, 1 m KCl(aq) and 4 m KCl(aq). Spectra a−c are recorded with the XAS technique, while spectra d−f are recorded with XRS. By using eq 7 and assuming that the variation of the chosen saturation compensating factor with respect to ϵ_f is negligible, the XAS spectra are compensated for the saturation effects and show the same peak-intensity ratios as the XRS spectra; see spectra g−i in Figure 3. The XAS spectra of water and aqueous solutions can thus successfully be compensated for saturation effects by using eq 7 with a selected C'' independent of ϵ_f.

To visualize the compensation procedure and its sensitivity to different detection depths, we show in Figure 4a the change in the intensity scale of the water XAS spectrum and in Figure 4b how different detection depths affect the deviation from the correct linear intensity−absorption relationship. Equation 3 indicates that a detection depth as low as 10 nm is necessary to obtain a recorded spectrum without any observable saturation effects. The detection depth in the current XAS experiment is estimated to be ca. 300 nm.[44] By comparing the corrected absorption spectra with the tabulated values of the oxygen absorption edge,[45] a rough estimation of the absorption coefficients at the pre-edge and the main-edge peaks can be obtained; see Figure 4a. The correlation between the tabulated values and the saturated XAS spectrum results in absorption coefficients of 23 100 cm^{-1} at the pre-edge and 55 100 cm^{-1} at the main-edge in a correct absorption spectrum (dash−dotted lines in Figure 4b). The corrected spectrum in Figure 4a indicates absorption coefficient values at the pre-edge and main-edge peaks of 21 700 and 54 600 cm^{-1}, respectively (dash−dotted lines in Figure 4a). It is thereby possible to compensate the saturated 300 nm curve in Figure 4b as much as the peak intensities in the corrected spectrum (Figure 4a) indicate. The close agreement between the saturated compensated intensity−absorption relationship and the correct linear intensity−absorption relationship, despite the unknown accuracy of the estimate of the detection depth and the lack of extended absorption region, is an indication of a successful procedure to compensate saturation effects; this has furthermore been carefully calibrated against the XRS spectra.

2.4. The XRS Experimental Technique. A bulk-sensitive alternative to soft X-ray XAS on low *Z* elements such as oxygen is nonresonant XRS.[22,46,47] At low-momentum transfer, XRS, which is the X-ray energy loss version of XAS, results in spectra identical to XAS.[25] The XRS measurements of liquid water and aqueous solutions were performed at the Bio-CAT beamline 18-ID at the Advanced Photon Source (APS) in Argonne, IL. XRS was analyzed with a high-resolution multicrystal Si(440) analyzer operated in Rowland geometry at a Bragg angle of ∼88° which corresponds to an energy of 6462 eV. A lead-shielded liquid-N_2-cooled low-noise germanium detector was used to minimize background scattering signal not rejected by the analyzer. The Ge detector signal was normalized to the incident photon flux, I_0, recorded with a He-filled ion chamber. The O 1s XRS spectra were obtained by scanning the beamline Si(111) monochromator from 6980 to 7054 eV, with 0.1 eV steps in the near-edge region (6990−7015 eV) and 0.5 eV steps elsewhere. The total energy resolution of 1.0 eV was obtained by measuring the elastic scattering at 6462 eV. To avoid nondipole contributions, the spectra were taken at scattering angles below 78° corresponding to a momentum transfer of $q < 4$ $Å^{-1}$ (see Wernet et al.[20] supplemental material). XRS spectra were corrected for background from predominantly Compton scattering, by subtraction of an extrapolated function fitted to a region well below the absorption edge. Solutions were measured in a plastic cup with a hole covered with a 25-μm-thick Kapton window to reduce intensity loss of incident and scattered X-rays. The water spectrum was measured using a 5-mm-diameter plastic flow tube with a similar window. An earlier test using liquid water showed no difference between spectra obtained in a flow tube and a plastic container. Contributions from the Kapton window were subtracted using an empty cell spectrum. The XRS spectra were calibrated in energy with the pre-edge peak position taken from the calibrated O 1s XAS fluorescence yield measurements, and the spectra were normalized by area between 530 and 550 eV. For a detailed discussion of XRS applications, see for example, Bergmann et al.[47] and/or Krisch et al.[48]

2.5. Samples. The samples were prepared from commercially available salts from Sigma-Aldrich. Salt, sample notation, and concentration are presented in Table 2. The salts were dissolved in deionized water without any further preparations.

TABLE 2: Samples in the O 1s XA Study of Aqueous Solutions[a]

salt	sample notation	molality/[m]
deionized water	H_2O	55.5
sodium chloride, NaCl	NaCl(aq)	1.0
potassium chloride, KCl	KCl(aq)	1.0 and 4.0
aluminum chloride hexahydrate, $AlCl_3 \cdot 6H_2O$	$AlCl_3$(aq)	0.9 and 2.7

[a] The ion concentration in the aqueous solutions is in molality (m = mole of solute/kilogram of solvent) at 25 °C.

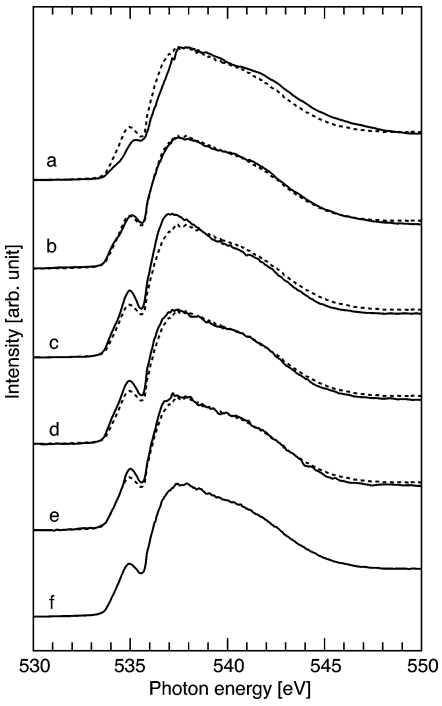

Figure 5. O 1s XA of (a) 2.7 m $AlCl_3$(aq), (b) 0.9 m $AlCl_3$(aq), (c) 4.0 m KCl(aq), (d) 1.0 m KCl(aq), (e) 1.0 m NaCl(aq), and (f) pure water. The 1.0 m NaCl(aq) and 1.0 m KCl(aq) spectra show small changes compared to the pure water spectrum (dotted), while the 4.0 m KCl(aq) spectrum shows larger changes. The 0.9 m $AlCl_3$(aq) spectrum shows a very small change compared to pure water (dotted), despite the fact that Al^{3+} is a strongly hydrated cation.

3. Results and Discussion

The selected cations in the solutions under investigation are sodium (Na^+), potassium (K^+), and aluminum (Al^{3+}). We chose chloride anion (Cl^-) as a counterion, since this ion has been reported to have no measurable effect on the HB network.[4,49] Na^+ and K^+ are neither strongly nor weakly hydrated and are assumed to have no significant effect on the HB network, while Al^{3+} is strongly hydrated and hence regarded to essentially influence the HB structure.[4−6] Figure 5d−f shows O 1s XA spectra of 1.0 m KCl(aq), 1.0 m NaCl(aq), and pure water, respectively; lower concentrations (<1 m) lead to insignificant changes in the main spectral features. To emphasize the spectral changes upon hydration of the ions, difference spectra between the solutions and pure water are shown in Figure 6 d,e. The difference spectra are multiplied by a factor of 3 to highlight the differences, which consist of a redistribution of the intensity from the high-energy region to the low-energy region. The amount of redistributed intensity is, however, very small, only 2.3% and 1.6% of the total pure water intensity below 550 eV for KCl(aq) and NaCl(aq), respectively. The increase in the pre- and main-edge peaks is an indication of an increase of SD configurations induced by the ions in the aqueous solution. The decrease in the low-energy part of the post-edge region (538.5−540 eV) indicates that there are specific structures of tetrahedral water that are modified to become SD species; the post-edge is associated with intact hydrogen bonds, and its position reflects the HB distance.[50] The shift of intensity from the low-energy post-edge region to lower energies thus indicates that hydrogen bonds that already have quite large distortions, corresponding to low post-edge energy, are turned into SD species.[20] The effects are, however, rather limited. The negligible effects at the higher post-edge energies indicate that hydrogen bonds that are still intact have the same length as a strong hydrogen bond in the pure water.

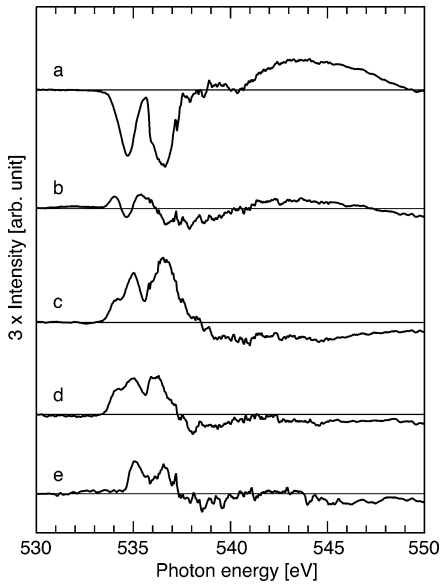

Figure 6. Difference XA spectra of aqueous solution minus pure water for (a) 2.7 m $AlCl_3$(aq), (b) 0.9 m $AlCl_3$(aq), (c) 4.0 m KCl(aq), (d) 1.0 m KCl(aq), and (e) 1.0 m NaCl(aq). The intensity is multiplied by a factor of 3 relative the intensity for all spectra in Figure 5. The positive peaks at 535 and 536.5 eV and the negative peak around 539 eV indicate an increase of SD configurations in NaCl(aq) and KCl(aq). The reverse trend is observed for $AlCl_3$(aq) including a shift of the spectral profile toward higher energies compared to the pure water spectrum.

Al^{3+} is a strongly hydrated cation that may form or break up bonds in the HB network. Figure 5b shows O 1s XA spectra of pure water and 0.9 m $AlCl_3$(aq), while the corresponding difference spectrum subtracting the pure water spectrum is shown in Figure 6b, multiplied by a factor of 3. If Al^{3+} has any bond-breaking/-making effect on the HB structure, we would see a clear difference between the XA spectra of 0.9 m $AlCl_3$(aq) and pure water, since more than 10% of the water molecules are solvation spheres of Al^{3+} and 30% are solvation spheres of Cl^-.[51] The effects are, however, very modest, and the difference spectrum gives an observed change of only 1.4% of the total pure water intensity below 550 eV, showing some decrease of SD species and an increase of tetrahedrally bonded molecules. The strong electric field of Al^{3+} might have been expected to shift the peak positions or affect the peak intensities in the XA spectra. A density functional theory (DFT) calculation indicates that the intensity of the pre-edge is not affected, but a shift to higher energies might occur,[52] which we actually also can see in the XA spectrum.

By comparing the trends in the XA spectra of the solutions, we might be able to evaluate the effect of the Cl^- ion or confirm that effects from Cl^- are not measurable by XAS/XRS. Although the 0.9 m $AlCl_3$(aq) solution has almost three times as much Cl^- as the 1.0 m NaCl(aq) or KCl(aq), the change of the XA spectrum, relative to pure water, is smaller: 1.4% versus 1.6% and 2.3%, respectively. Furthermore, the changes in the

spectra of NaCl(aq) and KCl(aq) are opposite to the changes in the spectrum of $AlCl_3$(aq). On the basis of the observed trends in the XA spectra of the solutions, we can thus exclude Cl^- as a source of the observed changes in the XA spectra; this is furthermore in agreement with earlier reports indicating that Cl^- does not have measurable effects on the HB network.[4,49]

The results indicate that there are structural changes in liquid water induced by solvated ions, but the spectral changes do not provide support either for a breakdown or for a buildup of the bulk HB network in the water. Earlier work has shown that a breakdown (buildup) of hydrogen bonds affect the XA spectra by redistributing intensity from (to) the post-edge region to (from) the pre-edge and main-edge region.[19−21] Although strongly hydrated ions are considered to severely influence the long-range HB structure in the bulk liquid, we observe a very weak structure-maker/structure-breaker effect of the HB network for the solutions near 1 m. The effect for $AlCl_3$(aq) is even weaker than the effect we observe for the comparatively weakly hydrated Na^+ and K^+ ions in terms of affecting the relative amounts of SD configurations and tetrahedrally coordinated waters. Na^+ and K^+ are considered to have no significant effect on the liquid bulk structure.[4−6] In a more general sense, we thus infer that the average number of hydrogen bonds in the bulk HB structure of water remains basically unchanged upon solvation of the ions.

There is also a difference between solutions of Al^{3+} ions and Na^+ and K^+ ions in terms of pH. Hydroxylation of the Al^{3+} ion results in a lowering of the pH due to the formation of Al−OH species. It is known from previous work that signatures of the OH species can be seen at energies below the pre-edge peak around 533−535 eV.[27] Since there is no observable intensity in that region in the spectra in Figure 5, the concentration of OH must be relatively small compared to the amount of water. Effects on the XA water spectral shape due to the presence of H^+ and OH^- in the solution are only seen for relatively high concentrations above 4 m.[53,54]

In the 4.0 m KC1(aq) and 2.7 m $AlCl_3$(aq) solutions, almost all water molecules are in the vicinity of an ion, and bulk water no longer exists in the solution. The spectral changes can therefore be considered as an effect of the interaction between the ions and the water molecules in the solvation sphere. The XA spectrum for 4.0 m KCl(aq) (see Figure 5c and highlighted in Figure 6c) shows an increase at the pre- and main-edge peaks and a decrease at the post-edge peak, whereas the opposite is seen in the XA spectrum for 2.7 m $AlCl_3$(aq) (Figure 5a and highlighted in Figure 6a). Those changes are ascribed to, respectively, an increase (KCl) and a decrease ($AlCl_3$) in the amount of SD species in the first solvation sphere of the respective ions. The amount of redistributed intensity is, however, still small: 3.8% and 4.6% of the total pure water intensity below 550 eV, respectively. The change in the post-edge, as seen in the difference spectra, spans a large energy range, indicating a decrease (KCl) and an increase ($AlCl_3$), respectively, of tetrahedrally coordinated water with many different HB distances and angles. The shift of the post-edge peak in the $AlCl_3$(aq) spectrum to higher energies may also indicate that the distance between the water molecules in the first and second solvation spheres is shorter than the average HB length in bulk water.

At very high ion concentrations, the majority of the water molecules are in the first solvation sphere of the ions. It is clearly indicated that, in the first solvation sphere of a strongly hydrated ion, water molecules have fewer broken hydrogen bonds than in pure bulk water. On the other hand, water molecules in the first solvation sphere of weakly hydrated ions have more broken hydrogen bonds. These results are in agreement with a neutron diffraction study that indicates a difference in the hydrogen-bond donating and accepting capacities of water in the first solvation sphere[9] and with recent time-resolved infrared spectroscopy studies where a change in the rotational dynamics of water is only seen in the first solvation sphere.[10,11] It is likely that the observed decrease and increase, respectively, of broken hydrogen bonds of water in the first solvation sphere can be related to some of the unique properties of water. However, with XAS/XRS, we are only probing changes in the HB network locally around the excited oxygen atom, and there can thus be other more subtle long-range changes in the water structure that XAS/XRS is not sensitive to.

4. Conclusions

The HB structure of water in the bulk and the first solvation sphere of ions is studied with XAS and XRS. A high concentration of ions (>1 m) is necessary before visual changes of the main spectral features occur in the recorded absorption spectra, which indicates that neither strongly nor weakly hydrated ions affect significantly the average number of hydrogen bonds in the bulk liquid as probed with XAS/XRS. There are changes in the recorded spectra reflecting the HB situation in the aqueous solution, but concentrations of 1 m or higher, where the majority of the water molecules are in direct contact with the solvated ions, are necessary to detect major changes in the spectra. Hence, only the water molecules in the first solvation sphere of ions are, in terms of HB configurations, affected by the presence of the ions. Water molecules in the first solvation sphere of strongly hydrated ions have fewer broken hydrogen bonds compared to liquid water, whereas those in the first solvation sphere of weakly hydrated ions have more. Our investigation shows that hydrated ions hardly change the local HB configuration in bulk liquid water. Although known macroscopic properties of 1 m solutions studied here are different from those of pure water, the average number of hydrogen bonds in the bulk HB network in these solutions is essentially the same as that of pure water. Therefore, the effects on the macroscopic properties of water cannot be explained on the basis of changes in the local HB coordination (i.e., making or breaking hydrogen bonds in the bulk liquid).

Acknowledgment. This work was supported by the Swedish Foundation for Strategic Research, Swedish Natural Science Research Council, BES (Chemical & Geosciences), DOE and National Science Foundation (US) grant CHE-0089215. The Advanced Light Source is supported by the Director, Office of Science, Office of Basic Energy Sciences, Material Sciences Division, of the U.S. Department of Energy under contract no. DE-AC03-76SF00098 at Lawrence Berkeley National Laboratory. Portions of this research were carried out at the Stanford Synchrotron Radiation Laboratory, a national user facility operated by Stanford University on behalf of the U.S. Department of Energy, Office of Basic Energy Sciences.

References and Notes

(1) Chowdhuri, S.; Chandra, A. *J. Chem. Phys.* **2003**, *118*, 9719.
(2) Korolev, N.; Lyubartsev, A. P.; Rupprecht, A.; Nordenskiöld, L. *Biophys. J.* **1999**, *77*, 2736.
(3) Saeger, W. *Principles of nucleic acid structure*; Springer-Verlag: New York, 1983.
(4) Collins, K. D.; Washabaugh, M. W. *Quart. Rev. Biophys.* **1985**, *18*, 323.
(5) Cacace, M. G.; Landau, E. M.; Ramsden, J. J. *Quart. Rev. Biophys.* **1997**, *30*, 241.

(6) Jenkins, H. D. B.; Marcus, Y. *Chem. Rev.* **1995**, *95*, 2695.
(7) Jones, G.; Dole. M. *J. Am. Chem. Soc.* **1929**, *51*, 2950.
(8) Krestov, G. A.; Myasnikov, E. R. *Thermodynamics of Solvation: Solution and Dissolution, Ions and Solvents, Structure and Energetics*; Ellis Horwood Series in Physical Chemistry; Ellis Horwood Ltd.: New York, 1990.
(9) Leberman, R.; Soper, A. K. *Nature (London)* **1995**, *378*, 364.
(10) Omta, A. W.; Kropman, M. F.; Woutersen, S.; Bakker, H. J. *Science* **2003**, *301*, 347.
(11) Omta, A. W.; Kropman, M. F.; Woutersen, S.; Bakker, H. J. *J. Chem. Phys.* **2003**, *119*, 12457.
(12) Chandrasekhar, J.; Jorgensen, W. L. *J. Chem. Phys.* **1982**, *77*, 5080.
(13) Obst, S.; Bradaczek, H. *J. Phys. Chem.* **1996**, *100*, 15677.
(14) Tongraar, A.; Liedl, K. R.; Rode, B. M. *J. Phys. Chem. A* **1998**, *102*, 10340.
(15) Chandrasekhar, J.; Spellmeier, D. C.; Jorgensen, W. L. *J. Am. Chem. Soc.* **1984**, *106*, 903.
(16) Zhu, S.-B.; Robinson, G. W. *J. Chem. Phys.* **1992**, *97*, 4336.
(17) White, J. A.; Schwegler, E.; Galli, G.; Gygi, F. *J. Chem. Phys.* **2000**, *113*, 4668.
(18) Lightstone, F. C.; Schwegler, E.; Hood, R. Q.; Gygi, F.; Galli, G. *Chem. Phys. Lett.* **2001**, *343*, 549.
(19) Myneni, S.; Luo, Y.; Näslund, L-Å.; Cavalleri, M.; Ojamäe, L.; Ogasawara, H.; Pelmenschikov, A.; Wernet, Ph.; Väterlein, P.; Heske, C.; Hussain, Z.; Pettersson, L. G. M.; Nilsson, A. *J. Phys.: Condens. Matter* **2002**, *14*, L213.
(20) Wernet, Ph.; Nordlund, D.; Bergmann, U.; Cavalleri, M.; Odelius, M.; Ogasawara, H.; Näslund, L.-Å.; Hirsch, T. K.; Ojamäe, L.; Glatzel, P.; Pettersson, L. G. M.; Nilsson, A. *Science* **2004**, *304*, 995.
(21) Cavalleri, M.; Ogasawara, H.; Pettersson, L. G. M.; Nilsson, A. *Chem. Phys. Lett.* **2002**, *364*, 363.
(22) Bergmann, U.; Wernet, Ph.; Glatzel, P.; Cavalleri, M.; Pettersson, L. G. M.; Nilsson, A.; Cramer, S. P. *Phys. Rev. B* **2002**, *66*, 092107.
(23) Bluhm, H.; Ogletree, D. F.; Fadley, C. S.; Hussain, Z.; Salmeron, M. *J. Phys.: Condens. Matter* **2002**, *14*, L227.
(24) Stöhr, J. *NEXAFS spectroscopy*; Springer-Verlag: New York, 1992.
(25) Näslund, L.-Å.; Lüning, J.; Ufuktepe, Y.; Ogasawara, H.; Wernet, Ph.; Bergmann, U.; Pettersson, L. G. M.; Nilsson, A. *J. Phys. Chem. B*, in press.
(26) Guo, J.-H.; Luo, Y.; Augustsson, A.; Rubensson, J.-E.; Såthe, C.; Ågren, H.; Siegbahn, H.; Nordgren, J. *Phys. Rev. Lett.* **2002**, *89*, 137402.
(27) Näslund, L.-Å.; Cavalleri, M.; Ogasawara, H.; Nilsson, A.; Pettersson, L. G. M.; Wernet, Ph.; Edwards, D. C.; Sandström, M.; Myneni, S. *J. Phys. Chem. A* **2003**, *107*, 6869.
(28) Wilson, K. R.; Cavalleri, M.; Rude, B. S.; Schaller, R. D.; Nilsson, A.; Pettersson, L. G. M.; Goldman, N.; Catalano, T.; Bozek, J. D.; Saykally, R. J. *J. Phys.: Condens. Matter* **2002**, *14*, L221.
(29) Odelius, M.; Ogasawara, H.; Nordlund, D.; Fuchs, O.; Weinhardt, L.; Maier, F.; Umbach, E.; Heske, C.; Zubavichus, Y.; Grunze, M.; Denlinger, J. D.; Pettersson, L. G. M.; Nilsson, A. *Phys. Rev. Lett.* In press.
(30) Tröger, L.; Arvanitis, D.; Baberschke, K.; Michaelis, H.; Grimm, U.; Zschech, E. *Phys. Rev. B* **1992**, *46*, 3283.
(31) Eisebitt, S.; Böske, T.; Rubensson, J.-E.; Eberhardt, W. *Phys. Rev. B* **1993**, *47*, 14103.
(32) Wight, G. R.; Brion, C. E. *J. Electron Spectrosc. Relat. Phenom.* **1974**, *4*, 25.
(33) Ishii, I.; McLaren, R.; Hitchcook, A. P.; Robin, M. B. *J. Chem. Phys.* **1987**, *87*, 4344.
(34) Nilsson, A.; Palmer, R. E.; Tillborg, H.; Hernnäs, B.; Guest, R. J.; Mårtensson, N. *Phys. Rev. Lett.* **1992**, *68*, 982.
(35) Puglia, C.; Nilsson, A.; Hernnäs, B.; Karis, O.; Bennich, P.; Mårtensson, N. *Surf. Sci.* **1995**, *342*, 119.
(36) Domke, M.; Mandel, T.; Puschmann, A.; Xue, C.; Shirley, D. A.; Kaindl, G.; Petersen, H.; Kuske, P. *Rev. Sci. Instrum.* **1992**, *63*, 80.
(37) Nilsson, A.; Björneholm, O.; Zdansky, E. O. F.; Tillborg, H.; Mårtensson, N.; Andersen, J. N.; Nyholm, R. *Chem. Phys. Lett.* **1992**, *197*, 12.
(38) Kim, D. Y.; Lee, K.; Ma, C. I.; Mahalingam, M.; Hanson, D. M. *J. Chem. Phys.* **1992**, *97*, 5915.
(39) Schirmer, J.; Trofimov, A. B.; Randall, K. J.; Feldhaus, J.; Bradshaw, A. M.; Ma, Y.; Chen, C. T.; Sette, F. *Phys. Rev. B* **1993**, *47*, 1136.
(40) Hunter-Dunn, J.; Arvanitis, D.; Mårtensson, N.; Tischer, M.; May, F.; Russo, M.; Baberschke, K. *J. Phys.: Condens. Matter* **1995**, *7*, 1111.
(41) Nakajima, R.; Stöhr, J.; Idzerda, Y. U. *Phys. Rev. B* **1999**, *59*, 6421.
(42) Regan, T. J.; Ohldag, H.; Stamm, C.; Nolting, F.; Lüning, J.; Stöhr, J.; White, R. L. *Phys. Rev. B* **2001**, *64*, 214422.
(43) Lüning, J.; Nolting, F.; Scholl, A.; Ohldag, H.; Seo, J. W.; Fompeyrine, J.; Locquet, J.-P.; Stöhr, J. *Phys. Rev. B* **2003**, *67*, 214433.
(44) Näslund, L.-Å. Probing unoccupied electronic states in aqueous solutions. Doctoral Thesis, Stockholm University, 2004; ISBN 91-7265-974.2. Available at http://www.diva-portal.org/su/theses/abstract.xsql?dbid=294.
(45) Henke, B. L.; Gullikson, E. M.; Davis, J. C. *At. Data Nucl. Data Tables* **1993**, *54*, 181. See also www-cxro.lbl.gov/optical_constants/.
(46) Bowron, D. T.; Krisch, M. H.; Barnes, A. C.; Finney, J. L.; Kaprola A.; Lorenzen, M. *Phys. Rev. B* **2000**, *62*, R9223.
(47) Bergmann, U.; Glatzel, P.; Cramer, S. P. *Microchem. J.* **2002**, *71*, 221 and references therein.
(48) Krisch, M.; Sette, F. *Surf. Rev. Lett.* **2002**, *9*, 969.
(49) Dutkiewicz, E.; Jakubowska, A. *ChemPhysChem* **2002**, *3*, 221.
(50) Odelius, M.; Cavalleri, M.; Nilsson, A.; Pettersson, L. G. M. *Phys. Rev. Lett.* Submitted for publication.
(51) Ohtaki, H.; Radnai, T. *Chem. Rev.* **1993**, *93*, 1157, and references therein.
(52) Näslund, L.-Å.; Odelius, M.; Pettersson, L. G. M.; Nilsson, A. Manuscript in preparation.
(53) Cavalleri, M.; Näslund, L.-Å.; Edwards, D. C.; Wernet, Ph.; Ogasawara, H.; Myneni, S., Ojamäe, L.; Nilsson, A.; Pettersson, L. G. M. Manuscript in preparation.
(54) Näslund, L.-Å.; Odelius, M.; Edwards, D. C.; Ogasawara, H.; Wernet, Ph.; Myneni, S.; Pettersson, L. G. M.; Nilsson, A. Manuscript in preparation.